Carotid Artery Calcium Score

Definition, classification, application, and limits

Abstract

Introduction: In the current paper the "carotid artery calcium score" method is presented with the target to offer a metric method to quantify the amount of calcification in the carotid artery.

Model and definition: The Volume of Interest (VOI) should be extracted and those voxels, with a Hounsfield Unit (HU) value ≥ 130, should be considered. The total weight value is determined by calculating the sum of the HU attenuation values of all voxels with values ≥ 130 HU. This value should be multiplied by the conversion factor ("or voxel size") and divided by a weighting factor, the attenuation threshold to consider a voxel as calcified (and therefore 130 HU): this equation determines the *Carotid Artery Calcium Score (CACS)*.

Results: In order to provide the demonstration of the potential feasibility of the model, the CACS was calculated in 131 subjects (94 males; mean age 72.7 years) for 235 carotid arteries (in 27 subjects unilateral plaque was present) considered. The CACS value ranged from 0.67 to 11716. A statistically significant correlation was found (rho value = 0.663, p value = 0.0001) between the CACS in the right and left carotid plaques. Moreover, a statistically significant correlation between the age and the total CACS was present (rho value = 0.244, p value = 0.005) whereas no statistically significant difference was found in the distribution of CACS by gender (p = 0.148). The CACS was also tested at baseline and after contrast and no statistically significant difference was found.

Conclusion: In conclusion, this method is of easy application, and it weights at the same time the volume and the degree of calcification in a unique parameter. This method needs to be tested to verify

its potential utility, similar to the coronary artery calcium score, for the risk stratification of the occurrence of cerebrovascular events of the anterior circulation. Further studies using this new diagnostic tool to determine the prognostic value of carotid calcium quantification are needed.

Introduction and rationale

Atherosclerosis of the carotid artery represents one of the key elements for the development of cerebrovascular events[1,2]. In the past few years significant efforts have been made to identify those features related to the risk of cerebrovascular events[3]. The atherosclerotic process is highly complex and varied, with different presentations among individuals due to a combination of genetic and environmental factors that activate various atherosclerotic pathways[4,5]. Calcium is an excellent target for identification among various features and tissues due to its strong attenuation effect on x-rays and the capability to serve as a quantitative imaging biomarker less prone to individual reader ascertainment bias[6]. Therefore, leveraging the ability of Computed Tomography (CT) to accurately detect calcifications, several recent papers have explored the impact of calcium and its amount and configuration for plaque protection and/or vulnerability[7–10]. Despite this active investigation on the role of carotid artery calcification on CT, there is an unmet need to standardize approaches to quantify and characterize calcium burden in individual patients.

The coronary arteries, like the carotid arteries, share similar pathobiological pathways and have been extensively studied in terms of the impact of calcium[11]. The Agatston Score, also known as the Coronary Artery Calcium Score, was developed in the 1990s to quantify the impact of calcium in the coronary arteries. This score measures the presence and severity of calcifications in the coronary arterial vasculature[12].

This metric has been widely utilized in recent years to evaluate the risk of Major Adverse Cardiac Events (MACE), as a low Agatston Score has been linked to a reduced likelihood of cardiovascular events and a high Agatston Score has a stronger association with a higher risk of such events[13,14]. The Agatston Score has become increasingly crucial in the risk stratification process through cardiovascular imaging[15,16].

The use of a comparable metric system for the assessment of calcium in the carotid arteries has historically posed challenges, as the automatic extraction of calcium components in this vessel is more complex than in the coronary artery due to the presence of other tissue with high Hounsfield

Units (HU). However, with the advancement of automatic segmenting systems, the extraction of voxel-based compositions is becoming increasingly facilitated[17], allowing for the potential implementation of a simplified method for the assessment of carotid artery calcium.

Hence, the development of a metric system reflecting the amount and density of calcium in the carotid artery could be a promising addition to the current risk stratification methods for predicting cerebrovascular events in the anterior circulation. This paper outlines the definition, mathematical model, and metrics behind the Carotid Artery Calcium Score (CACS), along with its potential uses and limitations.

Theoretical Method for the Carotid Artery Calcium Score calculation

- *DATA EXTRACTION*

Data extraction scenario 1 from noncontrast CT: In this scenario, the segmentation of plaques is not feasible as the inner boundary of the carotid artery plaque (luminal surface) cannot be distinguished without opacifying the lumen. However, there is no need to trace the plaque in detail, just the outer border of the plaque is sufficient, as all calcified voxels are considered part of the atherosclerotic process, by definition. After extracting the Volume of Interest (VOI), it must be evaluated and only voxels with a HU threshold value ≥ 130 HU should be considered (refer to **Figure 1** and **Figure 2**). Then, the next step is to perform the Metric Calculation.

Data extraction scenario 2: from contrast enhancement CT. Accurately segmenting the carotid artery plaque is crucial in this process. To ensure precise analysis of the plaque's calcium, it is essential to avoid any areas contaminated by contrast material and to take care in avoiding also halo and edge blur artifacts[18]. "Edge blur" refers to the transition or crispness of the outer boundary of the lumen in proportion to its diameter. "Halo" artifacts refer to the increased attenuation around the

lumen (partially saturated pixels). After successful extraction of the plaque, the VOI can be assessed and the next step, Metric Calculation, can proceed (as shown in **Figure 1**).

Data extraction scenario 3: from "virtual" noncontrast CT: The method applied in virtual noncontrast CT scans is identical to the process used in the data extraction scenario 2 from the noncontrast CT scans.

- *METRIC CALCULATION*

The VOI is made up of a varying number of voxels, which depends on the volume extracted. The HU values of each voxel in the VOI can be viewed in a column format (**Table 1**), where it is possible to see the HU attenuation value for each voxel. It is also possible to see the number of voxels that have each HU value. For the purpose of this analysis, which is to assess the calcium score, only those voxels with a HU value ≥ 130 should be considered, as per the HU classification proposed by De Weert and colleagues in 2006[19].

By considering only voxels with a threshold value of ≥130 HU, the number of calcified voxels and their HU values in the VOI can be determined. However, this only provides a count of the calcified voxels and does not take into account the varying degrees of density of the calcification, which can range from 130 to over 1000 HU.

It is clear (as shown in **Table 1**) that simply counting the number of calcified voxels alone doesn't account for their differing levels of calcification, represented by the HU attenuation values ranging from 130 to over 1000. To consider the impact of the varying degrees of calcification and their effect on attenuation, the contribution of each HU class must be considered. This can be achieved by calculating the **total weighted value**, which is the sum of the number of voxels multiplied by the HU of each contribution class, or simply by summing the HU attenuation values of all voxels with a value ≥ 130 HU.

total weighted value = sum of the number of voxels multiplied by the HU of each contribution class (≥ 130 HU)

or

total weighted value = summing the HU attenuation values of all voxels with a value ≥ 130 HU

- ***CONVERSION FACTOR (SIZE normalization) and WEIGHTING***

The last step is to normalize the result based on the size of the voxel, which can vary depending on factors such as the matrix size, length, and slice thickness. To do this, the total weighted value (sum of number of voxels * HU of each contribution class) must be multiplied by a conversion factor that depends on these parameters and then divided by the weighting factor (the HU threshold value of 130 used to identify a voxel as calcified). This weighting allows for comparison between voxels with different HU values, as 2 voxels with a value of 130 HU are equivalent to 1 voxel with a value of 260 HU. The result is the Carotid Artery Calcium Score.

Carotid artery calcium score = (total weighted value * voxel size)/130

Material and Methods

Demography

For the purpose of this analysis, 131 consecutive subjects (94 males; mean age 72.7 years) obtained from 2 centers (University of Cagliari – Italy and Mayo Clinic – Rochester USA) were studied using CT by calculating the CACS from non-contrast scans in 80 cases and from postcontrast scans in 51 cases. The analysis conducted on the population had the sole purpose of testing the potential technical application of the model, and therefore the analyses were not performed to study the relationships between CACS, demographic (excluding age and gender) and/or biological parameters, and/or outcomes, for which specific and targeted studies are referred to.

Plaque definition and model of analysis

The spatial limits we consider are those given by the plaque itself. Generally, plaques are localized in the distal tract of the CCA, extend to the bifurcation, and involve the ICA and the origin of the ECA. In order to define a reproducible method, we have always considered the last 4 centimeters of the CCA and the first 4 cm of the ICA and ECA. In this study, to extract the HU values of the ROI/ VOI form the data matrix, the free software Horos (version 3.3.6) was used. The traced ROI/VOI were exported as XML file where these HU data are visible. The data were then exported to Excel where, through a specially built work macro, the CACS values were generated.

Statistical analysis

The normality of each continuous variable group was tested using Kolmogorov-Smirnov *Z* test and Shapiro-Wilk. Continuous data were described as mean ± SD and binary variables were summarized as count (percentage). Correlation coefficients (Pearson rho product moment) were calculated between left and right CACS for gender. Intra-class correlation coefficients were also calculated. Mann-Whitney analysis was also calculated to test the differences between the groups. A p value < 0.05 was regarded to indicate statistical significance and all correlation values were calculated using a two-tailed significance level. *R* software (www.r-project.org) was employed for statistical analyses.

Results:

Demographic data

The CACS was calculated in 235 carotid arteries (in 27 subjects only unilateral plaque was present) from the cohort of 131 patients. In 100% of the cases, the plaques had metrically smaller dimensions (last 4 cm of CCA and first 4 cm of ICA and ECA) and always remained contained within

these spatial limits. The normality distribution was rejected using both Kolmogorov-Smirnov and Shapiro Wilk (**supplemental table 1** and **Supplemental Figure 1**). The descriptive data of the CACS are given in the **Table 2**.

The lowest value we have obtained was 0.67 whereas the highest was 11716.

Correlation analysis

A statistically significant correlation (rho value = 0.663, p value = 0.0001) between the CACS in the right and the left side was found, and this positive correlation was confirmed by groups (gender and type of scans) (**Figure 3**). Moreover, a statistically significant correlation between the age and the total CACS was present (rho value = 0.244, p value = 0.005) (**Supplemental Figure 2**).

Comparison between groups and reproducibility.

Due to the non-Gaussian distribution of the data, the Mann-Whitney test was used, and no statistically significant difference was found in the distribution of CACS by gender (p = 0.148). Similarly, no statistically significant difference was found in the distribution of the right CACS by gender (p = 0.402). A statistically significant difference was found, by gender for the CACS in the left carotid artery (p = 0.022) (**Supplemental Figure 3**). We also tested the CACS at baseline and after contrast to assess if the contrast influences the CACS results and the Mann-Whitney test showed no statistically significant difference. In subset of 20 patients (34 carotid plaques) the intra-class correlation coefficient (ICC) was calculated after re-test and the values shows almost identical results (**supplemental table 2)**.

Discussion:

It is crucial to identify features of plaques that may be linked to the prediction of cerebrovascular events in order to select the most effective therapeutic strategy[3]. In the past, the only

factor considered for therapeutic options was the degree of stenosis, however, increasing evidence suggests that plaque characteristics could greatly impact this area. There have been several recent efforts to analyze calcification, particularly in terms of type and configuration[7,9,20,21]. Despite these efforts, no current consensus exists on the optimal method to determine carotid artery calcium burden in a given patient, with most approaches used in the literature to date reliant on expert observations that may be difficult to reproduce in general clinical practice.

The simple measure of the amount of calcification, similar to the coronary artery calcium score, has not been widely adopted in carotid arteries[2]. It is important to note that the physiopathology of cerebrovascular events is different from that of myocardial infarcts, as most of the latter are caused by coronary artery pathology while only a portion of ischemic strokes are caused by atherosclerotic carotid artery disease. Nonetheless, finding a method to better stratify the risk of carotid-related cerebrovascular events remains important and there is evidence that the degree of calcification quantified using the Agatston method may be useful in predicting the clinical behavior of carotid plaques[22].

In the past, the segmentation of carotid arteries was considered to be a time-consuming task. However, with the development of automated models using advanced Artificial Intelligence (AI) carotid artery plaque segmentation has become a technically feasible and efficient option[17,23]. Additionally, the CACS can now be quickly obtained through noncontrast scan or using advanced CT technologies such as dual energy CT (DECT) and photon-counting CT (PCCT) which can create "virtual" noncontrast images[24]. This allows for easier extraction and the option of using a noncontrast scan rather than a post-contrast scan in certain situations. The use of noncontrast scans can also be beneficial in the context of a noncontrast cranial scan, as it allows for the inclusion of information related to the CACS.

Calcified voxels can have HU attenuation values from 130 to 2000 HU or greater. In each carotid plaque, varying degrees of calcific density may exist within the plaque and represented in each voxel. By summarizing the entire plaque, the varying calcific degree is not captured. Our method

captures both total volume and varying degrees of calcific density in one metric. In a radiology-pathology correlation study published in 2004, a strong and significant correlation between the calcium content of carotid plaques in carotid specimen and calcium measured by CT in vivo using the method[25] was measured (p value <0.001, rho value=0.969), suggesting radiographic measurements can be equivalent to histologic measurements.

A key point is the difference of the method we are presenting with the Agatston's method. Basically, there are 2 main conceptual differences: In the Agatston method[12] the calcium was defined as a "*radiation attenuating structure with a density of more than 130 Hounsfield units (HU) in an area of 1 square mm*". In other papers this value was changed (e.g. at least 0.5 square mm[25]). This represents a potential bias because it does not take into account the presence of punctiform or small size calcification patterns that could be a potential marker of pathology[26,27]. Moreover, as demonstrated in a recently published paper that applied the Agatston's method in the carotid artery for the calcium quantification, the method requires that the operator "select the cluster of calcium" to be considered and even if the inter-observer reproducibility is high[28] it does not maximize all of the available quantitative information.

The second difference is that the Agatston's method for the calculation of the calcium score is calculated as the product of the lesion area and the cofactor 1–4 (cofactor 1, 130–199 HU; cofactor 2, 200–299 HU, cofactor 3, 300–399 HU, cofactor 4≥400 HU). The cofactor is obtained considering the maximal computed tomographic number of each region of interest recorded. In the method we are suggesting we do not consider the class but the mathematical contribution of all voxels with an HU attenuation value >130 HU.

It would also be possible to consider the volume of calcium components (by calculating the volume of all voxels with an HU attenuation value > 130), as done in several papers[6,29,30] but this approach would not consider the different range of calcification that a voxel could have (and with the HU value that be significantly higher than 130 HU).

After creating the theoretical framework of CACS, we decided to test its feasibility in two separate populations to observe its real-world application. We selected 131 patients (235 carotids) to be analyzed using our CACS model. The application is straightforward as it simply involves identifying a region of space from which information needs to be extracted. In the case of the baseline study, circular regions of interest (ROIs) can be used, and on contrast-enhanced acquisitions, plaque segmentation analyses are performed. However, these methods are currently very rapid and efficient using algorithms that automatically extract the regions of space for analysis.

The distribution analysis (**supplemental Table 1**) showed that the calcium distribution is non-gaussian with most of the plaques that have CACS in the lower classes. Another interesting point we can identify from the data analysis is that there is no plaque that shows a CACS = 0. There are some sides where there is no calcific plaque (and in this case there is a virtual "0" value but in all the cases where a plaque was present, a small amount of calcium was also identified with a minimum value of 0.67. On the other hand, the highest absolute value was 11,716, indicating a difference of over 17.500 times between the smallest and largest values. This suggests that there is an extremely high dynamic range in the application of our CACS model.

Another implication of this analysis is that it is not possible to translate the concept of a "zero" coronary calcium score[31 32] to the carotid artery because, based on this cohort, all carotid arteries with any visualized plaque concurrently showed some calcifications and resulted in a CACS value above zero.

A further finding was that no statistically significant difference was found in CACS at baseline and after contrast. However, it is important to underline that this is a comparison between 2 distinct populations and further studies assessing the impact of the contrast in the same patients before and after contrast material or on virtual noncontrast and contrast-enhanced CTs should be done to validate this concept.

In this study the software Horos was used where it is possible to export the traced ROI/VOI as XML file where these HU data are included. However, regarding this point, it is useful to explain

that having the attenuation values of the voxels is sufficient, and for simplicity, we used the method described through Horos, but the entire process can be easily automated starting from the numerical data of the attenuations from all software that export this kind of data.

It is important to note some limitations in the application of this method. One of these limitations is the potential presence of calcium outside of the carotid artery bifurcation, such as in the proximal common carotid artery or distal internal carotid artery. The method described above does not account for the potential presence of atherosclerosis in these areas outside of the carotid bifurcation. This may result in an incomplete calculation of the calcium burden in the carotid arteries. However, this is considered a minor limitation as it is widely recognized that the carotid bifurcation is the most frequent and representative location for atherosclerosis involving the carotid artery.

The second limitation pertains to the energy used in analysis. In the examples given, a 120 kV energy parameter was used. However, it is widely known that energy levels impact photoelectric and Compton interactions and thus, HU attenuation. This limitation is considered minor, as shown in Blobel's coronary artery calcium score, where kV values did not significantly change CAC scoring values[33]. New dual energy and photon counting technologies eliminate this issue as they allow for specific energy levels to be selected in post-processing[34]. A third limitation that should be considered is that by considering the carotid artery plaque as the target of the calcium score, we are restricting the prediction range only to the anterior circulation. Feasibility and analyses of CACS for the posterior circulation need further evaluation. Another limitation is that CACS may not be able to capture the differences attributable to calcium morphology. For example, dense/nodular calcification may have a different implication than small, punctate calcification with the latter possible a marker of actively inflamed plaque. It may be necessary to couple CACS with inspection for certain calcium phenotypes that may confer different risk, also by considering the new metric model for the assessment of the carotid artery plaque[35].

In conclusion, we introduce Carotid Artery Calcium Score methodology, its derivation, and show feasibility. Its effectiveness requires further evaluation and validation, similar to the widely

accepted coronary artery calcium score for risk stratification in the incidence of cerebrovascular events in the anterior circulation. Future research utilizing this new diagnostic tool to assess the prognostic significance of accurate carotid calcium quantification is imperative and will enhance our understanding of the role of calcium in carotid plaque pathology.

References

1. Tsao CW, Aday AW, Almarzooq ZI, et al. *Heart Disease and Stroke Statistics-2022 Update: A Report from the American Heart Association*. Vol 145.; 2022. doi:10.1161/CIR.0000000000001052
2. Kleindorfer DO, Towfighi A, Chaturvedi S, et al. *2021 Guideline for the Prevention of Stroke in Patients with Stroke and Transient Ischemic Attack; A Guideline from the American Heart Association/American Stroke Association*.; 2021. doi:10.1161/STR.0000000000000375
3. Saba L, Saam T, Jäger HR, et al. Imaging biomarkers of vulnerable carotid plaques for stroke risk prediction and their potential clinical implications. *Lancet Neurol*. 2019;4422(19):1-14. doi:10.1016/S1474-4422(19)30035-3
4. Virmani R, Ladich ER, Burke AP, Kolodgie FD. Histopathology of carotid atherosclerotic disease. *Neurosurgery*. 2006;59(5 SUPPL.):219-227. doi:10.1227/01.NEU.0000239895.00373.E4
5. Larose E, Yeghiazarians Y, Libby P, et al. Characterization of human atherosclerotic plaques by intravascular magnetic resonance imaging. *Circulation*. 2005;112(15):2324-2331. doi:10.1161/CIRCULATIONAHA.105.538942
6. Baradaran H, Ng CR, Gupta A, et al. Extracranial internal carotid artery calcium volume measurement using computer tomography. *International Angiology*. 2017;36(5). doi:10.23736/S0392-9590.17.03811-1
7. Saba L, Chen H, Cau R, et al. Impact Analysis of Different CT Configurations of Carotid Artery Plaque Calcifications on Cerebrovascular Events. *AJNR Am J Neuroradiol*. 2022;43(2):272-279. doi:10.3174/ajnr.A7401
8. Saba L, Sanagala SS, Gupta SK, et al. Ultrasound-based internal carotid artery plaque characterization using deep learning paradigm on a supercomputer: a cardiovascular disease/stroke risk assessment system. *International Journal of Cardiovascular Imaging*. Published online 2021. doi:10.1007/s10554-020-02124-9
9. Yang J, Pan X, Zhang B, et al. Superficial and multiple calcifications and ulceration associate with intraplaque hemorrhage in the carotid atherosclerotic plaque. *Eur Radiol*. 2018;28(12):4968-4977. doi:10.1007/s00330-018-5535-7
10. Pini R, Faggioli G, Fittipaldi S, et al. Relationship between Calcification and Vulnerability of the Carotid Plaques. *Ann Vasc Surg*. 2017;44:336-342. doi:10.1016/j.avsg.2017.04.017
11. Williams MC, Kwiecinski J, Doris M, et al. Low-Attenuation Noncalcified Plaque on Coronary Computed Tomography Angiography Predicts Myocardial Infarction: Results From the Multicenter SCOT-HEART Trial (Scottish Computed Tomography of the HEART). *Circulation*. 2020;141(18):1452-1462. doi:10.1161/CIRCULATIONAHA.119.044720

12. Agatston AS, Janowitz WR, Hildner FJ, Zusmer NR, Viamonte M, Detrano R. Quantification of coronary artery calcium using ultrafast computed tomography. *J Am Coll Cardiol*. 1990;15(4):827-832. doi:10.1016/0735-1097(90)90282-T
13. Osborne-Grinter M, Kwiecinski J, Doris M, et al. Association of coronary artery calcium score with qualitatively and quantitatively assessed adverse plaque on coronary CT angiography in the SCOT-HEART trial. *Eur Heart J Cardiovasc Imaging*. 2022;23(9):1210-1221. doi:10.1093/ehjci/jeab135
14. Budoff MJ, Mayrhofer T, Ferencik M, et al. Prognostic value of coronary artery calcium in the PROMISE study (Prospective Multicenter Imaging Study for Evaluation of Chest Pain). *Circulation*. 2017;136(21):1993-2005. doi:10.1161/CIRCULATIONAHA.117.030578
15. Mortensen MB, Gaur S, Frimmer A, et al. Association of Age with the Diagnostic Value of Coronary Artery Calcium Score for Ruling Out Coronary Stenosis in Symptomatic Patients. *JAMA Cardiol*. 2022;7(1):36-44. doi:10.1001/jamacardio.2021.4406
16. Peng AW, Dardari ZA, Blumenthal RS, et al. Very High Coronary Artery Calcium (≥1000) and Association with Cardiovascular Disease Events, Non–Cardiovascular Disease Outcomes, and Mortality: Results from MESA. *Circulation*. 2021;143(16):1571-1583. doi:10.1161/CIRCULATIONAHA.120.050545
17. Sheahan M, Ma X, Paik D, et al. Atherosclerotic Plaque Tissue: Noninvasive Quantitative Assessment of Characteristics with Software-aided Measurements from Conventional CT Angiography. *Radiology*. 2018;286(2):622-631. doi:10.1148/radiol.2017170127
18. Claves JL, Wise SW, Hopper KD, Tully D, Ten Have TR, Weaver J. Evaluation of contrast densities in the diagnosis of carotid stenosis by CT angiography. *American Journal of Roentgenology*. 1997;169(2):569-573. doi:10.2214/ajr.169.2.9242779
19. De Weert TT, Ouhlous M, Meijering E, et al. In vivo characterization and quantification of atherosclerotic carotid plaque components with multidetector computed tomography and histopathological correlation. *Arterioscler Thromb Vasc Biol*. 2006;26(10):2366-2372. doi:10.1161/01.ATV.0000240518.90124.57
20. Baradaran H, Eisenmenger LB, Hinckley PJ, et al. Optimal carotid plaque features on computed tomography angiography associated with ischemic stroke. *J Am Heart Assoc*. 2021;10(5):1-10. doi:10.1161/JAHA.120.019462
21. Toussaint JF, LaMuraglia GM, Southern JF, Fuster V, Kantor HL. Magnetic resonance images lipid, fibrous, calcified, hemorrhagic, and thrombotic components of human atherosclerosis in vivo. *Circulation*. 1996;94(5):932-938. doi:10.1161/01.CIR.94.5.932
22. Yoon WJ, Crisostomo P, Halandras P, Bechara CF, Aulivola B. The Use of the Agatston Calcium Score in Predicting Carotid Plaque Vulnerability. *Ann Vasc Surg*. 2019;54:22-26. doi:10.1016/j.avsg.2018.08.070
23. Murgia A, Balestrieri A, Francone M, et al. Plaque imaging volume analysis: technique and application. *Cardiovasc Diagn Ther*. 2020;10(4):1032-1047. doi:10.21037/cdt.2020.03.01
24. D'Angelo T, Albrecht MH, Caudo D, et al. Virtual non-calcium dual-energy CT: clinical applications. *Eur Radiol Exp*. 2021;5(1). doi:10.1186/s41747-021-00228-y
25. Denzel C, Lell M, Maak M, et al. Carotid artery calcium: Accuracy of a calcium score by computed tomography - An in vitro study with comparison to sonography and histology. *European Journal of Vascular and Endovascular Surgery*. 2004;28(2):214-220. doi:10.1016/j.ejvs.2004.05.004
26. Maldonado N, Kelly-Arnold A, Vengrenyuk Y, et al. A mechanistic analysis of the role of microcalcifications in atherosclerotic plaque stability: Potential implications for plaque rupture. *Am J Physiol Heart Circ Physiol*. 2012;303(5). doi:10.1152/ajpheart.00036.2012
27. Vengrenyuk Y, Carlier S, Xanthos S, et al. A hypothesis for vulnerable plaque rupture due to stress-induced debonding around cellular microcalcifications in thin fibrous caps. *Proc Natl Acad Sci U S A*. 2006;103(40):14678-14683. doi:10.1073/pnas.0606310103

28. Shenouda R, Vancheri S, Maria Bassi E, et al. The relationship between carotid and coronary calcification in patients with coronary artery disease. *Clin Physiol Funct Imaging*. 2021;41(3):271-280. doi:10.1111/cpf.12694
29. Moradi M, Mehdi M, Mahdavi B, Nogourani MK. The Relation of Calcium Volume Score and Stenosis of Carotid Artery. Published online 2020. doi:10.1016/j.jstrokecerebrovasdis.2019.104493
30. Saba L, Raz E, Grassi R, et al. Association between the volume of carotid artery plaque and its subcomponents and the volume of white matter lesions in patients selected for endarterectomy. *American Journal of Roentgenology*. 2013;201(5). doi:10.2214/AJR.12.10217
31. Blaha MJ, Cainzos-Achirica M, Greenland P, et al. Role of Coronary Artery Calcium Score of Zero and Other Negative Risk Markers for Cardiovascular Disease : the Multi-Ethnic Study of Atherosclerosis (MESA). *Circulation*. 2016;133(9):849-858. doi:10.1161/CIRCULATIONAHA.115.018524
32. Biavati F, Saba L, Boussoussou M, et al. Coronary Artery Calcium Score Predicts Major Adverse Cardiovascular Events in Stable Chest Pain. *Radiology*. 2024;310(3). doi:10.1148/radiol.231557
33. Blobel J, Mews J, Goatman KA, Schuijf JD, Overlaet W. Calibration of coronary calcium scores determined using iterative image reconstruction (AIDR 3D) at 120, 100, and 80 kVp. *Med Phys*. 2016;43(4):1921-1932. doi:10.1118/1.4942484
34. Mergen V, Higashigaito K, Allmendinger T, et al. Tube voltage-independent coronary calcium scoring on a first-generation dual-source photon-counting CT-a proof-of-principle phantom study. *Int J Cardiovasc Imaging*. 2021;38(4):905-912. doi:10.1007/S10554-021-02466-Y
35. Saba L, Cau R, Murgia A, et al. Carotid Plaque-RADS, a novel stroke risk classification system. *JACC Cardiovasc Imaging*. Published online September 29, 2023. doi:10.1016/j.jcmg.2023.09.005

Tables

Table 1

Case example 1			Case example 2			Case example 3		
HU scale	Number of Voxel	Weighted value	HU scale	Number of Voxel	Weighted value	HU scale	Number of Voxel	Weighted value
130	0	0	130	0	0	130	0	0
140	1	140	140	0	0	140	0	0
150	5	750	150	0	0	150	0	0
160	0	0	160	0	0	160	0	0
170	0	0	170	0	0	170	0	0
180	8	1440	180	0	0	180	0	0
190	0	0	190	0	0	190	0	0
200	12	2400	200	0	0	200	0	0
210	0	0	210	0	0	210	0	0
220	0	0	220	0	0	220	0	0
230	15	3450	230	0	0	230	0	0
240	0	0	240	0	0	240	0	0
250	0	0	250	0	0	250	0	0
260	17	4420	260	0	0	260	0	0
270	0	0	270	0	0	270	0	0
280	0	0	280	0	0	280	0	0
290	19	5510	290	0	0	290	0	0
300	0	0	300	0	0	300	0	0
310	21	6510	310	0	0	310	0	0
320	15	4800	320	0	0	320	0	0
330	0	0	330	0	0	330	0	0
340	0	0	340	0	0	340	0	0
350	15	5250	350	32	11200	350	0	0
360	0	0	360	44	15840	360	0	0
370	0	0	370	32	11840	370	0	0
380	32	12160	380	0	0	380	0	0
390	0	0	390	0	0	390	0	0
400	0	0	400	0	0	400	0	0
410	21	8610	410	0	0	410	0	0
420	0	0	420	0	0	420	0	0
430	0	0	430	0	0	430	0	0
440	0	0	440	0	0	440	0	0
450	45	20250	450	31	13950	450	31	13950
460	0	0	460	0	0	460	0	0
470	0	0	470	21	9870	470	21	9870
480	0	0	480	32	15360	480	32	15360
490	53	25970	490	43	21070	490	46	22540

500	0	0
510	0	0
Total voxel	**279**	**total weighted**
Media	**7,15**	**101660**

500	8	4000
510	36	18360
Total voxel	**279**	**total weighted**
Media	**7,15**	**121490**

500	65	32500
510	84	42840
Total voxel	**279**	**total weighted**
Media	**7,15**	**137660**

carotid artery Calcium score = **SUM of Number of voxels * HU of each Contribution Class * voxel size** / 130

CACS example 1	*CACS example 2*	*CACS example 3*
186.4	222.8	252.4

Table 1 legend: Example of CACS value distribution inf 3 different cases. In the tables the values ≥ 130 HU were considered and grouped according to the HU class. Even if in the three tables the total number of voxels is the same (279 voxels) the total weighted value is different due to the different distribution of the HU Classes. The CACS is therefore different in the three examples.

Descriptives		
	Statistic	*Std. Error*
Left CACS		
Mean	932,4096	*123,7157*
95% Confidence Interval for Mean		
Lower Bound	*687,617*	
Upper Bound	*1177,202*	
5% Trimmed Mean	726,0303	
Median	399,57	
Variance	1974418	
Std. Deviation	1405,14	
Minimum	0	
Maximum	8949,71	
Range	8949,71	
Interquartile Range	1155,48	
Skewness	2,751	*0,213*
Kurtosis	9,833	*0,423*
Right CACS		
Mean	882,8301	*109,8883*
95% Confidence Interval for Mean		
Lower Bound	*665,3973*	
Upper Bound	*1100,263*	
5% Trimmed Mean	710,6162	
Median	340,14	
Variance	1557732	
Std. Deviation	1248,091	
Minimum	0	
Maximum	5440,69	
Range	5440,69	
Interquartile Range	1145,23	
Skewness	2,005	*0,213*
Kurtosis	3,755	*0,423*
Total CACS		
Mean	1746,461	*216,4782*
95% Confidence Interval for Mean		
Lower Bound	*1318,122*	
Upper Bound	*2174,8*	
5% Trimmed Mean	1415,721	
Median	731,77	
Variance	6045304	
Std. Deviation	2458,72	
Minimum	0	
Maximum	11716,2	
Range	11716,2	
Interquartile Range	2607,1	
Skewness	2,061	*0,213*
Kurtosis	4,451	*0,423*

Table 2 legend: Descriptive statistics of CACS, total, right side, and left side.

Figure Legends

Figure 1: Panel A shows the acquisition of the ROI (performed using a circular ROI) in the area where the plaque is located. In panel B, the distribution of voxel attenuation values within this segmented region is shown as a histogram. Values below 130, which are below the threshold for being considered calcification, are not considered, and only values above 130 HU are included. Panels C and D depict the same process, but on an acquisition after contrast agent administration. In this case, since the attenuation of the contrast agent is above 130 HU and can be confused with that of calcified areas, the plaque needs to be segmented to exclude the contrast agent-affected regions. Once the ROI is identified, the distribution of attenuation values is displayed, and only values above 130 HU are selected.

Figure 2: The process of acquiring the ROI is demonstrated for each individual slice until plaque presence is identified (Panel A). The value of each ROI should then be summed to obtain the total CACS values. In Panel B, the number of calcified voxels detected in each individual slice is highlighted, along with the total contribution in terms of HU and the CACS value. This provides a slice-by-slice evaluation as well as the overall cumulative value.

Figure 3: Scatterplots (with regression line, solid black line, and 95% confidence intervals, dashed lines) are documented for the comparison between right and left sides, distributed by gender (Panel A) and by scan type (Panel B).

Figures

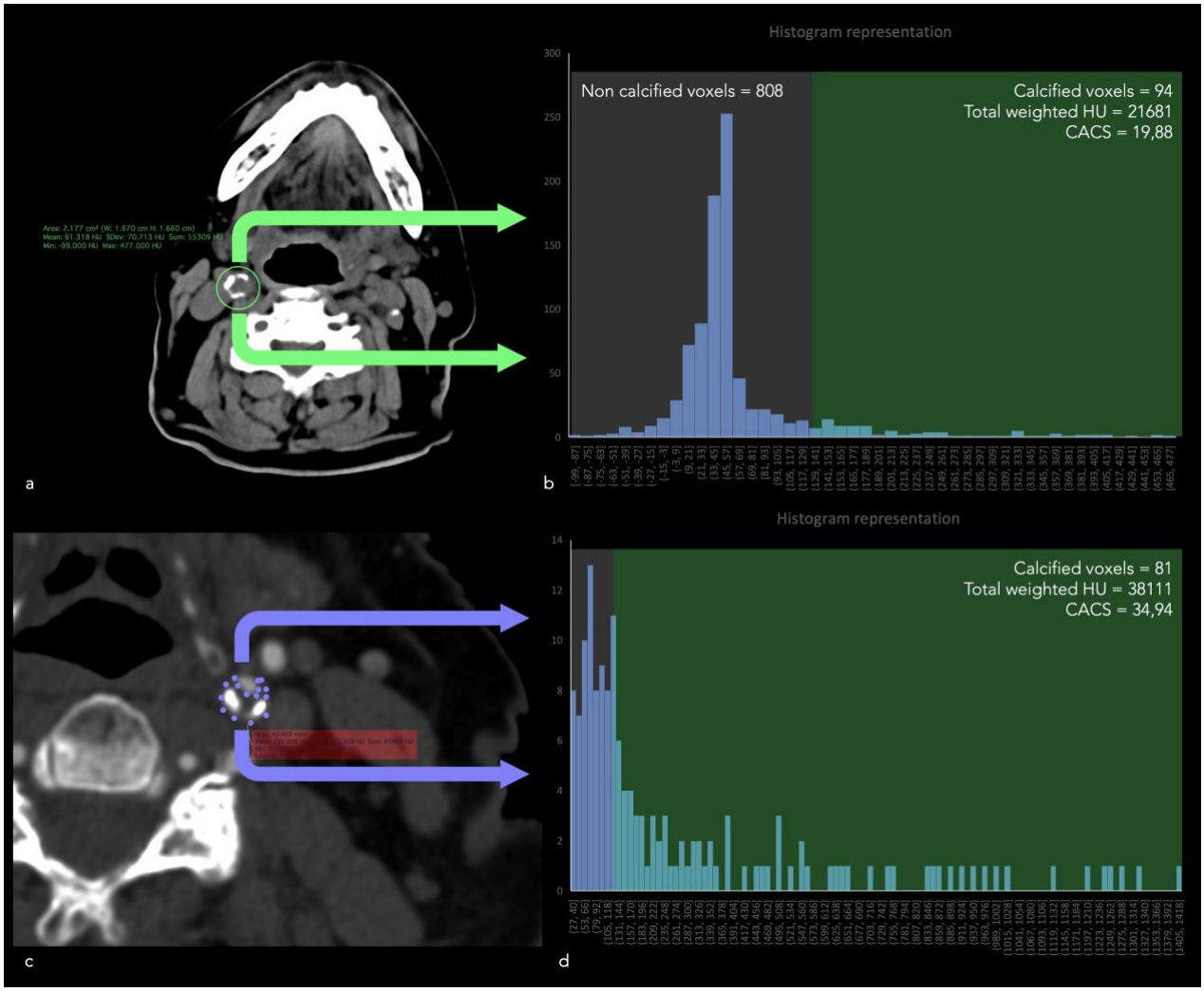

Figure 1: Panel A shows the acquisition of the ROI (performed using a circular ROI) in the area where the plaque is located. In panel B, the distribution of voxel attenuation values within this segmented region is shown as a histogram. Values below 130, which are below the threshold for being considered calcification, are not considered, and only values above 130 HU are included. Panels C and D depict the same process, but in an acquisition after contrast agent administration. In this case, since the attenuation of the contrast agent is above 130 HU and can be confused with that of calcified areas, the plaque needs to be segmented to exclude the contrast agent-affected regions. Once the ROI is identified, the distribution of attenuation values is displayed, and only values above 130 HU are selected.

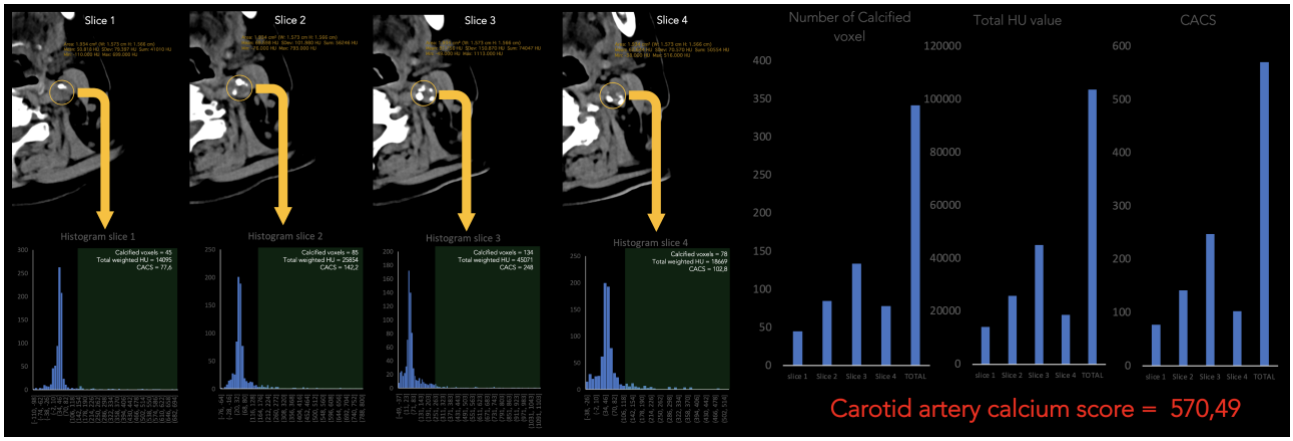

Figure 2: The process of acquiring the ROI is shown for each image slice until plaque presence is identified (Panel A). The value of each ROI should then be summed to obtain the total CACS values. In Panel B, the number of calcified voxels detected in each individual slice is highlighted, along with the total contribution in terms of HU and the CACS value. This provides a slice-by-slice evaluation as well as the overall cumulative value.

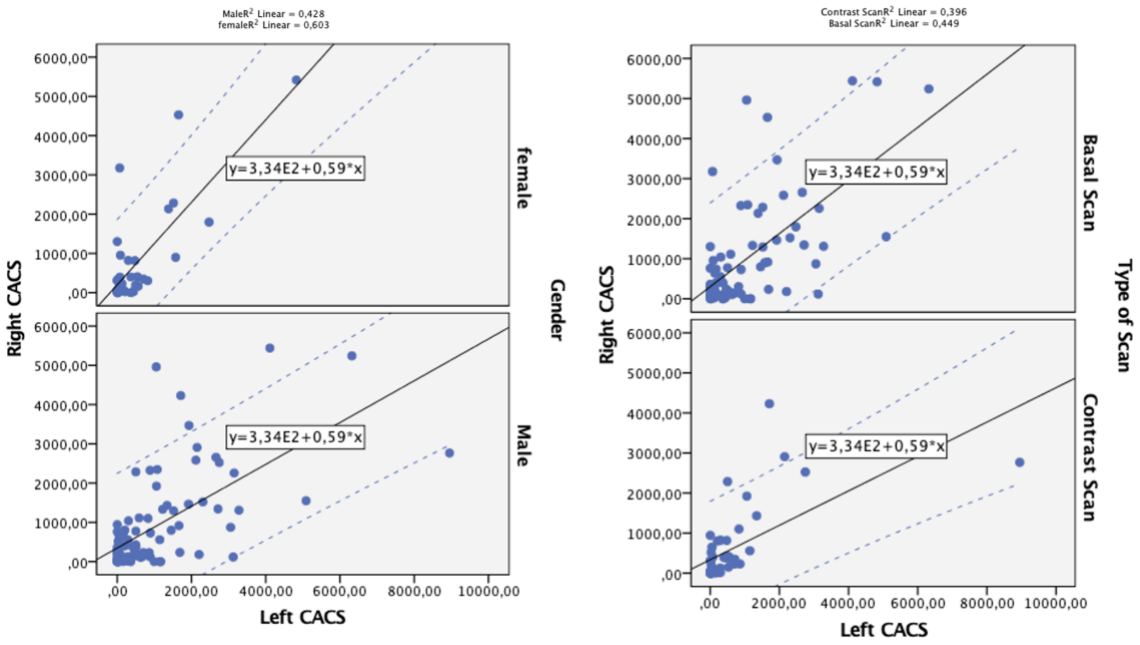

Figure 3: Scatterplots (with regression line, solid black line, and 95% confidence intervals, dashed lines) are documented for the comparison between right and left sides, distributed by gender (Panel A) and by scan type (Panel B).

Supplementary Table

TESTS OF NORMALITY

	Kolmogorov-Smirnov[a]			Shapiro-Wilk		
STATISTIC	Statistic	df	Sig.	Statistic	df	Sig.
LEFT CACS	0,253	129	0	0,678	129	0
RIGHT CACS	0,24	129	0	0,716	129	0
TOTAL CACS	0,251	129	0	0,724	129	0

A. LILLIEFORS SIGNIFICANCE CORRECTION

Supplementary Table 1: Normality test

Intraclass Correlation Coefficient

	Intraclass Correlation[b]	95% Confidence Interval		F Test with True Value 0			
		Lower Bound	Upper Bound	Value	df1	df2	Sig
Single Measures	1,000[a]	1,000	1,000	12221881,658	33	33	,
Average Measures	1,000[c]	1,000	1,000	12221881,658	33	33	,

Two-way mixed effects model where people effects are random and measures effects are fixed.

a. The estimator is the same, whether the interaction effect is present or not.

b. Type C intraclass correlation coefficients using a consistency definition. The between-measure variance is excluded from the denominator variance.

c. This estimate is computed assuming the interaction effect is absent, because it is not estimable otherwise.

Supplementary Table 2: Intraclass correlation coefficient in the subset of 20 patients

Supplementary Figures

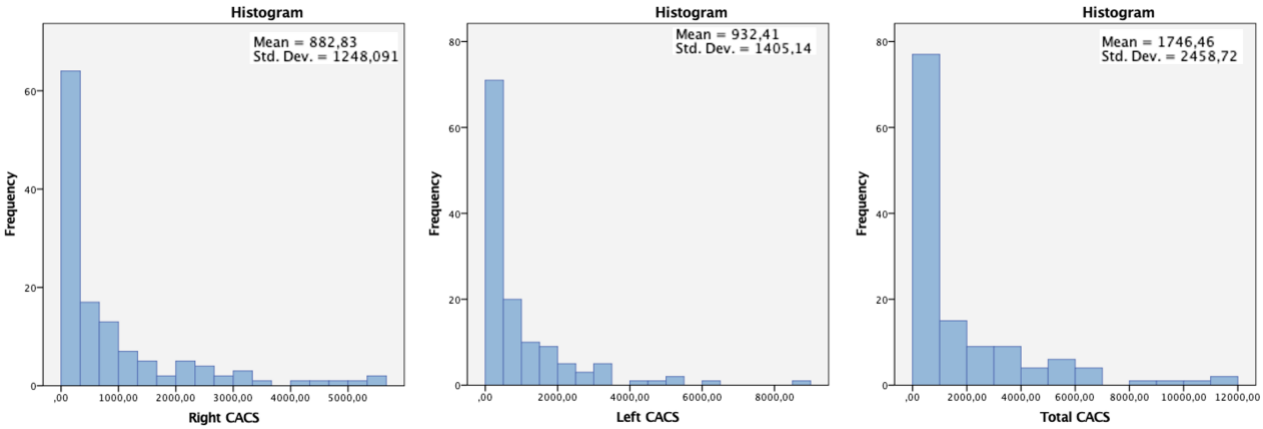

Supplementary Figure 1: Distribution of CACS in the cohort and according to the right and left side.

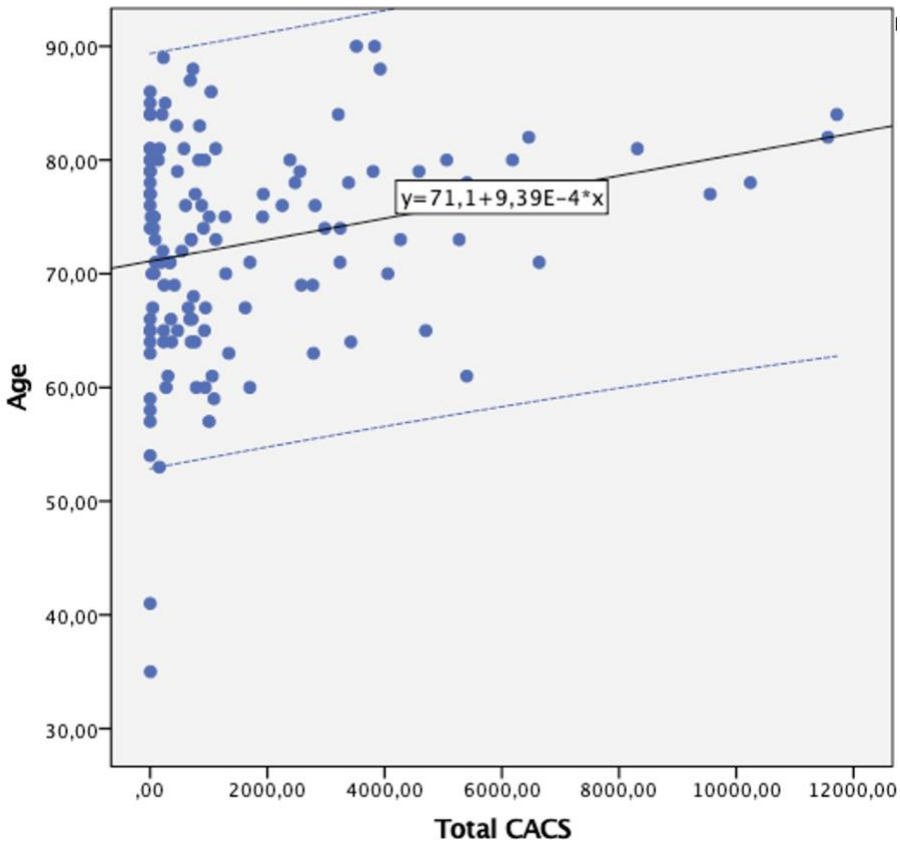

Supplementary Figure 2: Scatterplot (with regression line, solid black line, and 95% confidence intervals, dashed lines) are documented for the comparison between Total CACS and Age

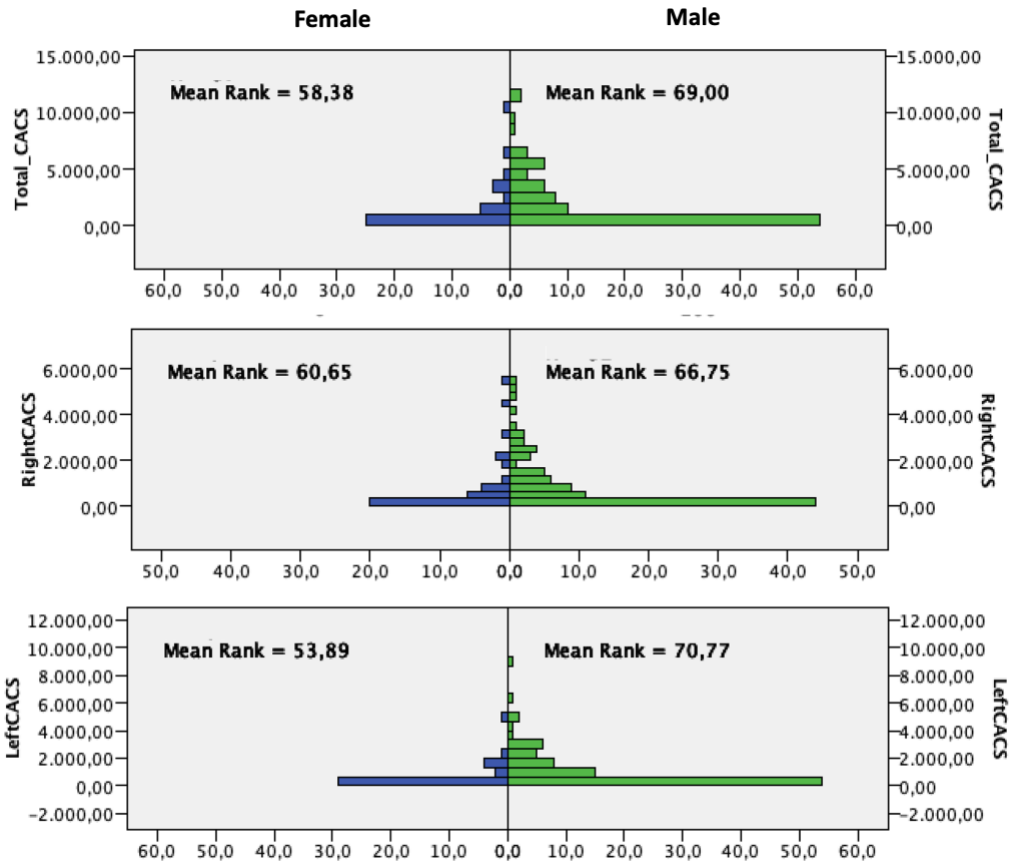

Supplementary Figure 3: CACS distribution by gender